Ascertaining the Limitations of Low Mobility on Organic Solar Cell Performance

B.M. Savoie*, S. Tan†, J.W. Jerome‡, C.-W.Shu†, M. A. Ratner*, T. J. Marks*
*Department of Chemistry, Northwestern University, Evanston, IL 60208 USA
e-mail: brettsavoie2014@u.northwestern.edu
†Division of Applied Mathematics, Brown University, Providence, RI 02912 USA
‡Department of Mathematics, Northwestern University, Evanston, IL 60208 USA

***Abstract*—In the past decade, organic photovoltaics (OPV) have emerged as an intensely studied alternative energy technology. The OPV platform presents several attractive qualities, yet, the high disorder and relative low mobility of the materials comprising OPV systems remain a bottleneck to further progress. We report here a modeling methodology that quantifies the efficiency losses engendered by the low mobility of these systems. We also report a methodology that explicitly treats the charge transfer (CT) state that has been shown to influence device performance. We compare two commonly studied OPV architectures, the bilayer (BL) and blended bulk-heterojunction (BHJ), and separately investigate the sensitivity of each architecture to mobility. Our findings suggest that mismatched mobilities of the active layer components can lead to additional recombination currents. We find that the collection current is largely limited by the slow carrier; consequently, the high mobility carriers only increase the recombination current without aiding collection.**

INTRODUCTION

The primary photoexcited species in OPVs are tightly bound excitons that must be subsequently separated at a donor-acceptor interface. The efforts of many researchers have focused on understanding this mechanism. However, more recently, collection related losses have come under increased scrutiny due to what are perceived to be anomalously low open circuit voltages (V_{OC}), fill factors (FF), and shunt resistance (R_{SH}) upon illumination. In addition, it has been observed that commonly optimized device thicknesses are shorter than the thickness required for complete light absorption, suggesting that the technology remains collection limited.

The specific problem of collection is to get carriers to the appropriate electrodes before recombination processes occur. The goal of this work is to quantify, through direct evaluation of the continuity and Poisson equations, the role of mobility and device architecture in collection related losses.

METHODOLOGY

Exciton (X), charge transfer state (I), electron (n) and hole (p) dynamics are treated within the traditional continuity equation framework (2-5), where the electric field (F) is treated self-consistently via Poisson's equation (1):

$$\varepsilon_0\varepsilon_r\frac{\partial F}{\partial x}=q(p(x)-n(x));\ F(x)=-\frac{\partial\phi}{\partial x} \tag{1}$$

$$\frac{\partial X}{\partial t}=G(x)-k_{cap}(x)X(x)+\frac{\mu_X k_B T_0}{q}\frac{\partial^2 X}{\partial x^2}-k_{R,X}X(x) \tag{2}$$

$$\frac{\partial I}{\partial t}=k_{cap}(x)X(x)-D(F,I,x)-k_{R,I}I(x) \tag{3}$$

$$\frac{\partial n}{\partial t}=D(F,I,x)-R(n,p)+\frac{\mu_n}{q}\frac{\partial}{\partial x}\left[qnF+k_B T_0\frac{\partial n}{\partial x}\right] \tag{4}$$

$$\frac{\partial p}{\partial t}=D(F,I,x)-R(n,p)-\frac{\mu_p}{q}\frac{\partial}{\partial x}\left[qpF-k_B T_0\frac{\partial p}{\partial x}\right] \tag{5}$$

The quantities *G*, *D*, and *R* are the exciton photogeneration rate, the exciton dissociation rate, and the carrier recombination rate, respectively. *G* is determined by the experimental photon flux under the assumption of exponential (Beer-Lambert) absorption, *D* is modeled using Braun's adaptation of Onsager's theory of geminate dissociation, and *R* is the traditional Langevin bimolecular recombination rate. The μ terms are the mobilities for species as designated by the subscripts.

$$D(F,I)=\frac{3\mu_{Eff}q}{4\pi\varepsilon_0\varepsilon_r a^3}\exp\left(-\frac{E_B}{k_B T_0}\right)\Phi(b)I(x) \tag{6}$$

$$G(x)=\alpha_0\Gamma_0 e^{-\alpha_0 x} \tag{7}$$

$$R(n,p)=\frac{q(\mu_n+\mu_p)np}{\varepsilon_0\varepsilon_r} \tag{8}$$

Here μ_{Eff} is the effective mobility, *a* is the thermalization radius, ε_r is the relative dielectric constant, E_b is the CT-state binding energy, Φ(b) is the Bessel function of order one, $b = q^3F/(8\pi\varepsilon_r\varepsilon_0 k_B^2 T_0^2)$, *F* is the electric field, and T_0 is the temperature. In (6), μ_{Eff} is distinguished from the bulk mobilities for electrons and holes (μ_n and μ_p), since it is generally necessary to use a much larger value for μ_{Eff} to match experimental photocurrents. In (7), α_0 is the absorption

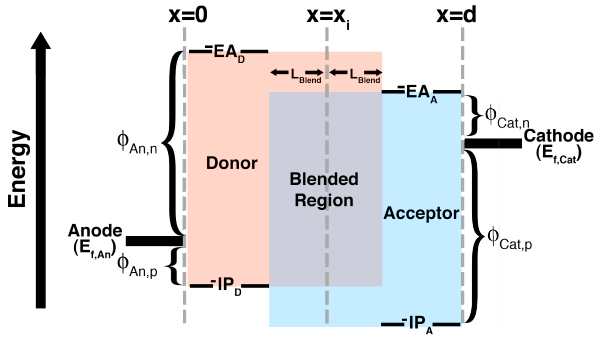

Fig. 1. Schematic depiction of the spatial dimensions and relevant energies employed in the model.

coefficient and Γ_0 is the incident photon flux. (8) is the standard expression for Langevin recombination.

Explicit incorporation of the CT state dynamics is unique to this study. Here, the exciton is permitted to decay into the interfacial CT species (I) at a rate k_{cap}, while k_{cap} is spatially only non-zero at interfacial regions. The physics of collection and exciton diffusion are captured through direct evaluation of the continuity equations. The dissociation phenomenology enters through treatment of the dissociation rate (here taken as Braun-Onsager [1]). The boundary conditions are employed as suggested by Scott and Malliaras, assuming a steady state equilibrium established by the hopping of carriers within image potential of the electrode [2].

Figure 1 shows the relevant dimensions and energies accounted for in the model, where $\phi_{An,n}$, $\phi_{An,p}$, $\phi_{Cat,n}$, $\phi_{Cat,p}$ are the injection barriers at the anode (An) and cathode (Cat) for electrons (n) and holes (p), respectively. The blended region is defined by the variable L_{Blend}. The approach permits direct gradation from the BL architecture to a BHJ architecture by varying L_{Blend}. Between the limits $L_{Blend} = 0$ and $L_{Blend} = d/2$, where d is the device thickness, the system moves between an idealized bilayer and bulk-heterojunction, this necessitates that the dielectric constant (ε) and k_{cap}, as discussed above, be spatially defined according to phase. Explicitly,

$$k_{cap}(x) = \begin{cases} 0 \;, & |x - x_i| > L_{Blend} \\ k_{cap,0} \;, & |x - x_i| \le L_{Blend} \end{cases} \qquad (9)$$

$$\varepsilon_r(x) = \begin{cases} \varepsilon_D, & 0 < x < x_i - L_{Blend} \\ \dfrac{\varepsilon_D + \varepsilon_A}{2} & |x - x_i| \le L_{Blend} \\ \varepsilon_A & x_i + L_{Blend} < x < d \end{cases} \qquad (10)$$

where the subscripts A and D refer to the value used in the donor and acceptor domains, respectively; x is the device depth measured from the anode, and ε_r is the relative dielectric constant.

For all simulations the mobilities and value of L_{Blend} are the only variables allowed to vary. The rest of the variables remain constant in all simulations and are defined in Table 1.

TABLE 1
Definitions and values of parameters used in the Study

Variable	**value**	***definition (units)***
ε_A	4	Relative dielectric in acceptor (unitless)
ε_D	3	Relative dielectric in donor (unitless)
T_0	300	Temperature (K)
$k_{cap,0}$	3×10^{12}	Exciton decay rate at interface (s^{-1})
$k_{R,I}$	10^9	Decay rate of CT species (s^{-1})
$k_{R,X}$	10^9	Decay rate of bulk exciton (s^{-1})
a	2×10^{-9}	Thermalization radius (m)
μ_{Eff}	10^{-5}	Effective mobility ($m^2V^{-1}s^{-1}$)
α_0	2×10^7	Absorption coefficient (m^{-1})
Γ_0	1×10^{21}	Photon flux ($photons \bullet m^{-2} \bullet s^{-1}$)
d	100×10^{-9}	Thickness (m)
L_D	10×10^{-9}	Exciton diffusion length (m)
τ_X	1×10^{-9}	Exciton lifetime (s)
$E_{f,An}$	-5	Workfunction of anode (eV)
$E_{f,Cat}$	-4	Workfunction of cathode (eV)
IP_D	5.25	Donor ionization potential (eV)
IP_A	6	Acceptor ionization potential (eV)
EA_D	3	Donor electron affinity (eV)
EA_A	3.75	Acceptor electron affinity (eV)
$N_{0,D}$	1×10^{27}	Electron density of states at Cathode (m^{-3})
$N_{0,A}$	1×10^{27}	Electron density of states at Anode (m^{-3})
$P_{0,D}$	1×10^{27}	Hole density of states at Anode (m^{-3})
$P_{0,A}$	1×10^{27}	Hole density of states at Cathode (m^{-3})

In our simulations we observed a numerical sensitivity to the value of k_{cap}. This is attributed to the different timescales of exciton dissociation and carrier transport that lead to a locally negative exciton population when the value of k_{cap} is set too high. The value of Γ_0 is taken to reflect that above bandgap photon flux for a poly(3-hexylthiophene) (P3HT) donor system matched with [6,6]-phenyl-C61-butyric acid methyl ester (PCBM) acceptor.

For numerical evaluation of Eqs. (1-5), we begin the evolution at zero values of the species and use third order accurate Runge-Kutta time stepping to reach steady state. The convection terms in the equations (4-5) are discretized by the fifth order weighted essentially non-oscillatory (WENO) finite difference method [3]. The second derivative terms are discretized by standard central differences. The combined algorithm allows us to use relatively coarse grids and still get very accurate results without any oscillation in the presence of sharp gradients or discontinuities in the solution.

This method builds on the work reported at the 14th IWCE[4]

DEVICE SIMULATION

A one-dimensional model is used, with a simulated device thickness of *100 nm*. Four series of simulations are conducted: two series on the BL architecture and two series on

the BHJ architecture. The BL architecture is treated by restricting D to take a non-zero value only at $x = d/2$, whereas the BHJ is simulated by permitting dissociation throughout the domain of x. This is achieved through the definition of k_{cap} in (9) as described above. The effect of mobility on device performance is investigated by varying the electron (μ_n) and hole mobility (μ_p) from 10^{-9} to 10^{-4} $m^2V^{-1}s^{-1}$ while holding them equal. The relative performance enhancements in the BL and BHJ architectures are reported. The effect of a mobility mismatch ($\mu_n \neq \mu_p$) is also investigated by taking $\mu_n = 10^{-9}$ $m^2V^{-1}s^{-1}$ while keeping $\mu_p = 10^{-4}$ $m^2V^{-1}s^{-1}$.

DISCUSSION

Figs. 2 and 3 show the simulations for the BL and BHJ systems, respectively, where the mobilities of both components are kept equal. It can be seen that both the BL and BHJ architectures see an improvement in carrier collection on moving to higher mobility, as evidenced by the improved FF in both sets of simulations. The overall effect of increasing mobility on the two sets of curves is very similar, and they are primarily only distinguished by the low current magnitudes of the BL series, which is a consequence of the incomplete exciton diffusion to the interface rather than collection losses. There are two notable features that bear explanation: severe shunt effects can be observed even at high mobility. This behavior is comparable to other studies using the assumption of bulk Langevin recombination. Actual devices generally show lower recombination, causing several authors to include a scaling factor [5]. It has been suggested that the lower observed rate is due to the partitioning of carriers in two phases in a real OPV device, whereas Langevin's result is derived for carriers in a single bulk. Second, there is a loss of V_{OC} with increasing mobility due to the dark injection of carriers. Interestingly, this effect results in a maximal mobility above which dark current and recombination via the Langevin term results in a net reduction of performance. Presently our model doesn't include the effect of blocking layers (Fig. 1), which may mitigate dark injection in real devices.

In general, the bilayer architecture is more robust to low mobility due to the smaller amount of interface, and consequently less opportunities for recombination. Similarly, the BL architecture shows a higher effective shunt resistance, indicating a lower overall Langevin loss. Of course, the overall current magnitude remains limited due to the large loss of excitons formed away from an interface. This balance suggests that some intermediate degree of mixing between the idealized BL and BHJ limits may be optimal [6].

We also conducted simulations to investigate the effect of a mobility mismatch on performance in both the BL and BHJ systems. The results are indicated in Figs. 4 and 5 for the BL and BHJ, respectively. Notably, for both the BL and BHJ simulations, the mobility mismatched simulations show lower overall performance than the mobility matched simulations. It should be noted that the simulations are performed using a modest mobility for the matched case (i.e. $\mu_n = \mu_p = 10^{-9}$ $m^2V^{-1}s^{-1}$) then *increasing* the mobility of one

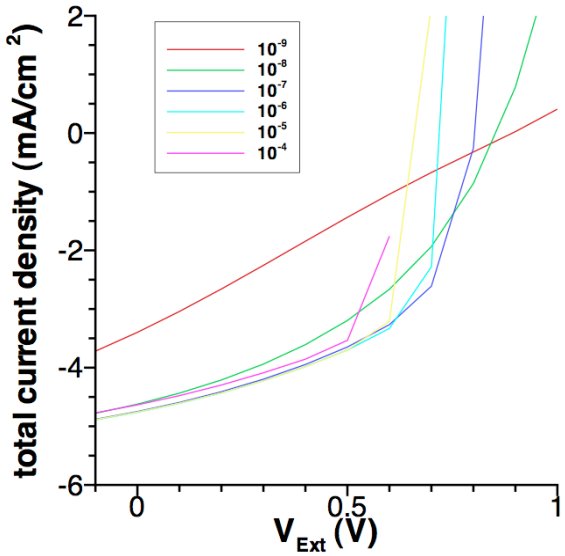

Fig. 2. Bilayer system simulations where $\mu_n = \mu_p$. The mobility is varied from $\mu = 10^{-9}$-10^{-4} $m^2V^{-1}s^{-1}$, d = 100 nm, and $\Gamma_0 = 10^{21}$ photons•$m^{-2}s^{-1}$. Optimal performance (as measured by the maximal product of $-V_{ext}$•J, where J is the current density) is obtained for the $\mu = 10^{-7}$ $m^2V^{-1}s^{-1}$ simulation. Increases in μ above 10^{-7} $m^2V^{-1}s^{-1}$, leads to reduced open circuit voltage (x intercept) due to dark current enhancement.

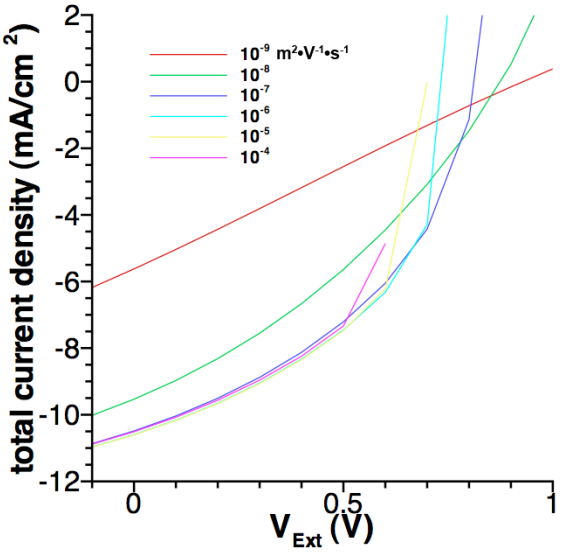

Fig. 3. Bulk Heterojunction system simulations where $\mu_n = \mu_p$. The mobility is varied from $\mu = 10^{-9}$-10^{-4} $m^2V^{-1}s^{-1}$, d = 100 nm, and $\Gamma_0 = 10^{21}$ photons•$m^{-2}s^{-1}$. The optimal mobility is found to be $\mu = 10^{-7}$ $m^2V^{-1}s^{-1}$. The BHJ shows a pronounced photocurrent enhancement at higher mobilities, accenting the important of langevin recombination in this architecture.

carrier for the mismatched simulation (i.e. $\mu_n = 10^{-4}$ $m^2V^{-1}s^{-1}$). We find the effect of increasing the mobility of just one carrier results in lower overall performance. We ascribe this behaviour to an increase in the recombination rate (via the Langevin mechanism) without a concomitant increase in collection rate due to space charge effects. At steady state, the current is

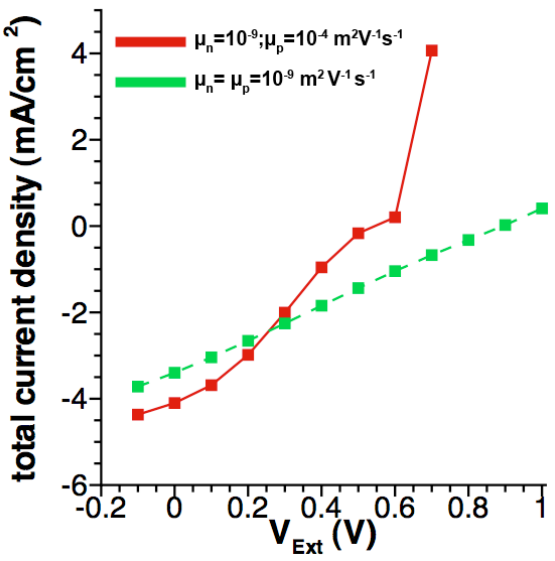

Fig. 4. Bilayer system simulations for $\mu_n \neq \mu_p$. Solid (Red): $\mu_n = 10^{-9}$ $m^2V^{-1}s^{-1}$ and $\mu_p = 10^{-4}$ $m^2V^{-1}s^{-1}$; Dashed (Green): $\mu_n = \mu_p = 10^{-9}$ $m^2V^{-1}s^{-1}$. Mismatched mobility results in an improved short-cicuit current (y-intercept) but leads to a compensating reduction in open circuit voltage (x-intercept).

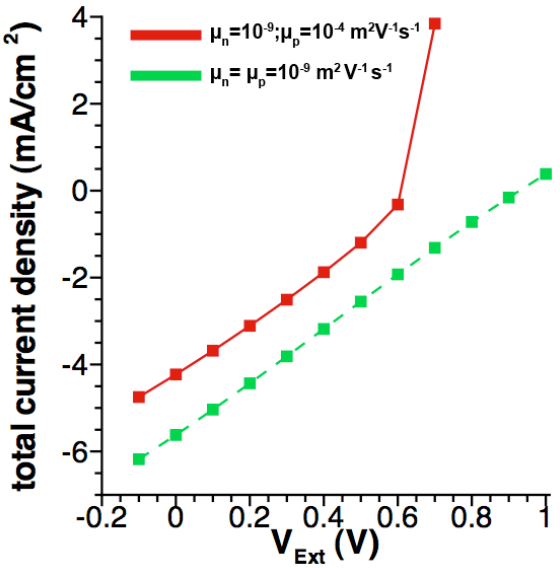

Fig. 5. Bulk heterojunction system simulations for $\mu_n \neq \mu_p$. Solid (Red): $\mu_n = 10^{-9}$ $m^2V^{-1}s^{-1}$ and $\mu_p = 10^{-4}$ $m^2V^{-1}s^{-1}$; Dashed (Green): $\mu_n = \mu_p = 10^{-9}$ $m^2V^{-1}s^{-1}$. Mismatched mobility results both open-circuit voltage (x-intercept) and photocurrent losses, unlike the bilayer system that showed some current enhancement.

largely limited by the slow carrier; this also limits the faster carriers' transit time through the device. In this situation the increased mobility only serves to increase the recombination rate and thus decrease performance. It is also notable that the BL architecture is less sensitive to the mismatch in mobility in comparison to the BHJ architecture. This is again indicative that it is the Langevin mechanism mediating the loss, since the BL architecture is in general less sensitive to Langevin losses, due to the limited amount of interface.

CONCLUSION

In conclusion, we report initial results from device simulations on BHJ and BL organic solar cell device architectures that investigate the role of mobility on overall performance. The direct numerical evaluation of the continuity equations allows us tremendous versatility in the systems we can simulate. In particular, it enables modelling of a continuum of device architectures between a pure bilayer and pure bulk-heterojunction. In the systems investigated we observe that the BHJ architecture is more sensitive to collection losses through the Langevin mechanism than the BJ architecture. This behaviour is observed in both the mobility matched and the mobility mismatched simulations. Notably, we find that mismatched mobilities of the active layer components can lead to additional recombination currents. We find that the collection current is largely limited by the slow carrier; consequently, the high mobility carriers only increase the recombination current without aiding collection. Our simulations also suggest that some intermediate architecture between the BHJ and BL may balance collection losses against exciton dissociation.

ACKNOWLEDGMENTS

B.M.S. thanks the Northwestern U. MRSEC for a predoctoral fellowship. NSF grant DMS-1112700 supported S. T. and C.-W.S. for this work. This work was supported as part of the ANSER Center, an Energy Frontier Research Center funded by the U.S. Department of Energy, Office of Science, Office of Basic Energy Sciences, under Award Number DE-SC0001059

REFERENCES

[1] C. Braun, "Electric field assisted dissociation of charge transfer states as a mechanism of photocarrier production," *J. Chem. Phys.,* Jan 1984.

[2] J. Scott and G. Malliaras, "Charge injection and recombination at the metal-organic interface," *Chem. Phys. Lett.,* vol. 299, pp. 115-119, Jan 1999.

[3] G. Jiang and C.-W. Shu, "Efficient implementation of weighted ENO schemes," *J. Comput. Phys.,* vol. 125, pp. 202-228, Jan 1996.

[4] J. Jerome, M. Ratner, J. Servaites, S. Tan, and C. -W, Shu, "Simulation of the Buxton-Clarke model for organic photovoltaic cells," *14th International Workshop on Computational Electronics,* Jan 2010.

[5] C. Deibel, A. Wagenpfahl, and V. Dyakonov, "Origin of reduced polaron recombination in organic semiconductor devices," *Phys. Rev. B,* vol. 80, p. 075203, Jan 2009.

[6] V. S. Gevaerts, L. J. A. Koster, M. M. Wienk, and R. A. J. Janssen, "Discriminating between Bilayer and Bulk Heterojunction Polymer: Fullerene Solar Cells Using the External Quantum Efficiency," *ACS Appl. Mater. Interfaces,* vol. 3, pp. 3252-3255, Jan 2011.